Statistical characteristics of polar cap mesospheric gravity waves observed by an all-sky airglow imager at Resolute Bay, Canada

S. Suzuki,[1] K. Shiokawa,[2] K. Hosokawa,[3] K. Nakamura,[4] and W. K. Hocking[5]

Received 30 July 2008; revised 20 September 2008; accepted 30 October 2008; published 29 January 2009.

[1] An airglow imager at Resolute Bay, Canada (74.7°N, 265.1°E) has been used for the observation of gravity waves in the polar cap mesosphere since January 2005. On the basis of the long-term imaging observations obtained over 137 nights during the winter seasons of 2005 and 2006, we extracted 143 events of small-scale (<100 km) gravity waves from sequential sodium airglow (589.3 nm) images. The observed waves typically had horizontal wavelengths of 20–50 km and phase speeds of 30–60 ms^{-1}. The propagation directions were predominantly westward. We also identified larger-scale (>100 km) gravity waves using airglow keograms, which represent a time series of the horizontal cross sections of the airglow images. The horizontal wavelengths and phase speeds of the large-scale waves were typically 100–400 km and 60–100 ms^{-1}, respectively. The propagation directions of these large-scale waves also showed a westward preference. The wave parameters appeared to have no relation with the geomagnetic activities represented by the K_p index. On the other hand, the propagation directions of the observed waves were consistent with the prevailing eastward winds in the mesosphere and the updraft associated with a low-pressure area that generally appears to the east of Resolute Bay at tropospheric altitudes. These results suggest that the main source of the gravity waves in the polar cap mesosphere is tropospheric dynamics rather than auroral activities.

Citation: Suzuki, S., K. Shiokawa, K. Hosokawa, K. Nakamura, and W. K. Hocking (2009), Statistical characteristics of polar cap mesospheric gravity waves observed by an all-sky airglow imager at Resolute Bay, Canada, *J. Geophys. Res.*, *114*, A01311, doi:10.1029/2008JA013652.

1. Introduction

[2] Airglow imaging has been widely used for the detection of gravity wave in the upper atmosphere since the 1990s owing to the development of highly sensitive charge-coupled device (CCD) detectors. This imaging technique is useful for investigating the two-dimensional (2-D) horizontal characteristics of small-scale (horizontal wavelength λ_h less than 100 km) gravity wave motions in the mesosphere and lower thermosphere (MLT); the gravity waves can be directly identified from sequential airglow images [e.g., *Taylor et al.*, 1995]. Gravity waves are known to contribute greatly to MLT dynamics through their dissipation, which is accompanied by the momentum transfer into the MLT mean flow [e.g., *Lindzen*, 1981; *Fritts and Alexander*, 2003].

[3] Since *Nakamura et al.* [1999] first made 18 months of imaging observations of small-scale gravity waves at Shigaraki (34.9°N, 136.1°E), Japan, several studies have reported on the seasonal and latitudinal/longitudinal variations in small-scale wave characteristics at various sites [e.g., *Nakamura et al.*, 2003; *Walterscheid et al.*, 1999; *Ejiri et al.*, 2003; *Suzuki et al.*, 2004; *Espy et al.*, 2004]. In particular, it was found that the horizontal propagation directions of gravity waves are dependent on the location where they are observed because the directions are greatly influenced by the wind/thermal conditions of the propagation paths and by the locations of the wave sources. The horizontal propagation direction is a key parameter for understanding the direction of mean flow acceleration (or deceleration) of the gravity waves.

[4] It has been reported that at the midlatitudes in the northern hemisphere, small-scale gravity waves tend to propagate eastward in summer and westward in winter; this suggests that the waves are filtered by the winds in the middle atmosphere in the zonal direction, which are westward in summer and eastward in winter [e.g., *Nakamura et al.*, 1999; *Ejiri et al.*, 2003; *Tang et al.*, 2005]. On the other hand, at the midlatitudes in the southern hemisphere and equatorial regions, the preferential directions of wave propagation are mostly in good agreement with the relative

[1] Sugadaira Space Radio Observatory, University of Electro-Communications, Chofu, Tokyo, Japan.
[2] Solar-Terrestrial Environment Laboratory, Nagoya University, Nagoya, Aichi, Japan.
[3] Department of Information and Communication Engineering, University of Electro-Communications, Chofu, Tokyo, Japan.
[4] Hydrospheric Atmospheric Research Center, Nagoya University, Nagoya, Aichi, Japan.
[5] Department of Physics and Astronomy, University of Western Ontario, London, Ontario, Canada.

0148-0227/09/2008JA013652

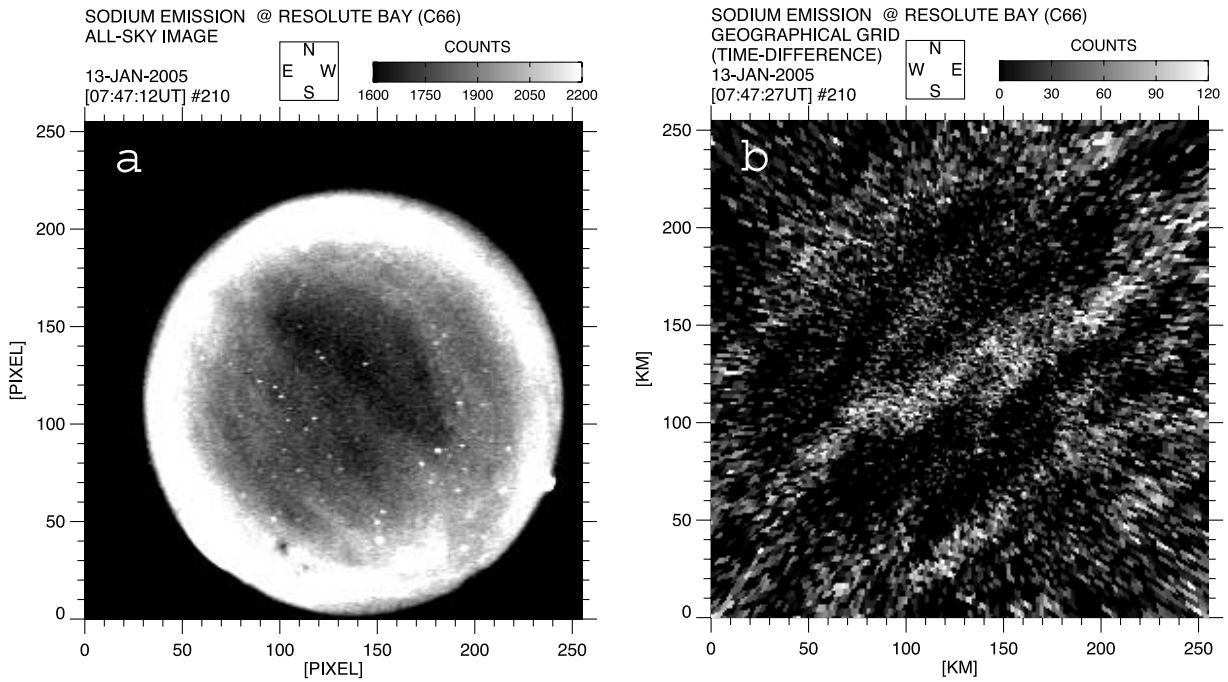

Figure 1. (a) Example of an all-sky sodium airglow image obtained at Resolute Bay, Canada, on 13 January 2005. The color scale is the sodium airglow intensity in unit of CCD count. (b) Same as Figure 1a, except for showing the time difference and the projection of the image onto a geographical grid of 256 × 256 km. The top and left of the image correspond to (a) the north and east directions and (b) the north and west directions, respectively.

locations of convection systems and the ducting structure at the MLT height rather than the wind filtering [*Nakamura et al.*, 2003; *Walterscheid et al.*, 1999; *Suzuki et al.*, 2004; *Wrasse et al.*, 2006].

[5] At high latitudes, relatively few imaging observations of gravity waves are obtained because of intense auroral emissions, which cause considerable contamination of the wave patterns in airglow images. At the same time, energy deposition processes associated with the auroral activity have been considered as possible wave sources [*Smith et al.*, 2000, and references therein].

[6] *Smith et al.* [2000] presented a study on gravity wave imaging observations obtained over 12 nights at Millstone Hill (42.6°N, 71.5°W), Massachusetts, in the subauroral zone. The results showed that there was no clear relation between the wave parameters (occurrence frequency and propagation direction) and geomagnetic activity (K_p index). *Espy et al.* [2004] showed that the momentum flux directions of small-scale gravity waves have a tendency to shift northwestward to southeastward; their results were based on the 79-night observation during the winters of 2000 and 2001 at Halley station, Antarctica (75.6°S, 26.6°W). These preferential directions were consistent with the filtering of waves by the stratospheric and lower mesospheric winds.

[7] In this paper, we report for the first time, the statistical characteristics of polar cap mesospheric gravity waves. The characteristics were determined using sodium airglow images obtained at Resolute Bay (74.7°N, 265.1°E, geomagnetic latitude: 82.9°), Canada during the winters of 2005 and 2006. In this region, a large climatological enhancement in stratospheric gravity wave variance, which could not be reproduced with a global mountain wave model, was observed by the microwave limb sounder on the Upper Atmosphere Research Satellite (UARS) [*Jiang et al.*, 2004]. We identified large-scale (λ_h > 100 km) gravity waves as well as conventional small-scale (λ_h < 100 km) gravity waves from the airglow images. To date, no statistical study of large-scale waves such as those observed in the MLT airglow images has been performed. We also discuss the possible sources of the observed polar cap gravity waves on the basis of the observed wave characteristics.

2. Observations

[8] The all-sky airglow imager at Resolute Bay has been operated since January 2005 as a one of the optical mesosphere thermosphere imagers (OMTIs) located there [*Shiokawa et al.*, 1999, 2009; *Hosokawa et al.*, 2006]. This imager has six interference filters on a rotating wheel, a fish-eye lens with a 180° field of view (FOV), and a cooled CCD camera with 512 × 512 pixels (note that, the imager installed at the Resolute Bay station was operated with 2 × 2 binning of all the CCD pixels, i.e., 256 × 256 pixels, in order to increase the output counts). In the present study, we used sodium emission images at a wavelength of 589.3 nm (typical emission height ∼90 km), which are obtained every 120 s with an exposure time of 30 s, since the sodium emission is least susceptible to auroral contamination [*Espy et al.*, 2004]. The optical imaging observations are made automatically during the period when the sun and moon are below the horizon with elevation angles of <−12° and <0°, respectively.

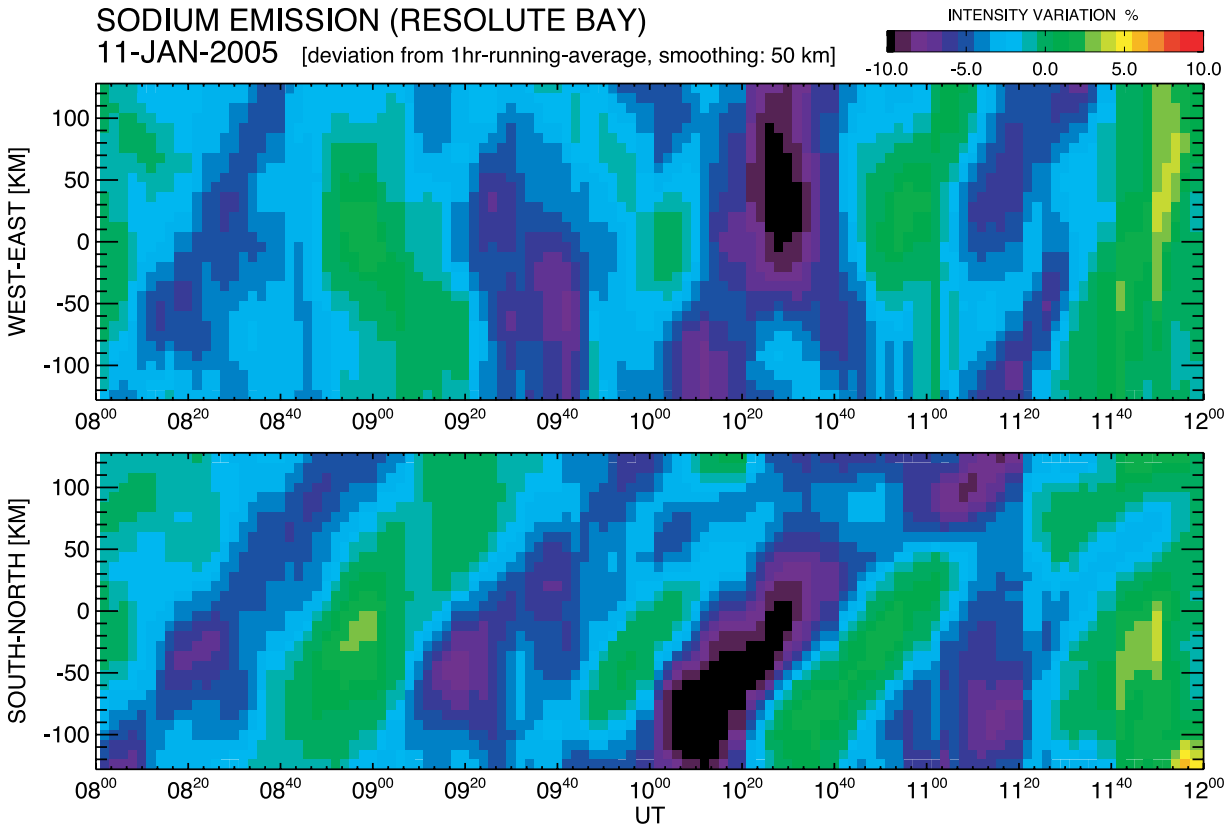

Figure 2. Intensity variations of sodium airglow in the (a) west–east and (b) north–south cross sections (keograms) for 0800–1200 UT on 11 January 2005. The intensity variations are defined as deviations from 1-hour running averages. Spatial smoothing with a size of 50 km was also performed for the keograms.

[9] Figure 1a shows an example of an all-sky sodium airglow image obtained at Resolute Bay on 13 January 2005 at 0747 UT. In order to investigate the wave structure in detail, the all-sky images were projected onto geographical coordinates with a size of 256 km × 256 km by assuming an emission height of 90 km, and then the time-difference images [*Swenson and Mende*, 1994] between consecutive images were calculated. Figure 1b is the processed image of Figure 1a. A southwest–northeast wave structure with a wavelength of ~40 km can be seen in the entire image. This conventional imaging process is often used to extract "small-scale gravity waves," whose 2-D characteristics (e.g., horizontal wavelength and phase speed) are identified directly in the imager's FOV.

[10] Figure 2 shows the west–east (top) and south–north (bottom) cross sections (keograms) of the sodium images, including the zenith pixel (location of Resolute Bay), for 0800–1200 UT on 13 January 2005. These keograms were developed by using the sodium images that were (1) projected onto the geographical grid as mentioned above, (2) taken as deviations from 1-hour running averages, and (3) smoothed spatially with a boxcar average of 50-km width. The imaging processes were based on the method introduced by *Shiokawa et al.* [2009], in which mesospheric airglow keograms were used to investigate the correspondence of mesospheric gravity waves to the waves in the thermosphere (ionosphere). In Figure 2, northwestward moving waves with a wave period of ~56 min are seen throughout the interval. The amplitude in the airglow intensity of ~5% was a typical value in this method. We investigated the characteristics of these "large-scale gravity waves" in the keograms as well as the small-scale waves.

[11] Figure 3 gives the sampling distribution of the imaging observations for the period from 9 January 2005

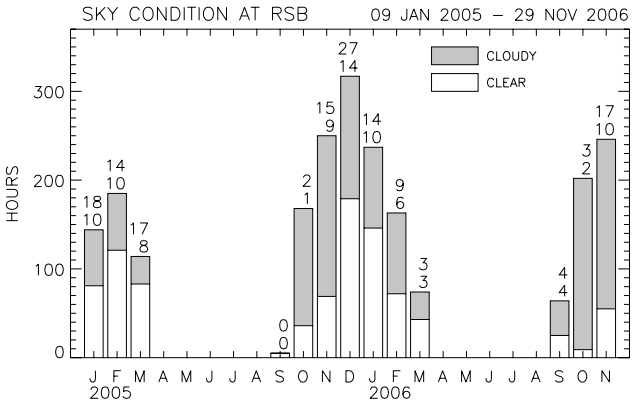

Figure 3. Monthly sampling distribution of the imaging observations at Resolute Bay from 9 January 2005 to 29 November 2006. The observation intervals are divided into clear-sky and cloudy conditions. Only the airglow images obtained for the clear-sky conditions were used in the present analysis. The numbers of events of small-scale (top) and large-scale (bottom) waves are shown above the histogram.

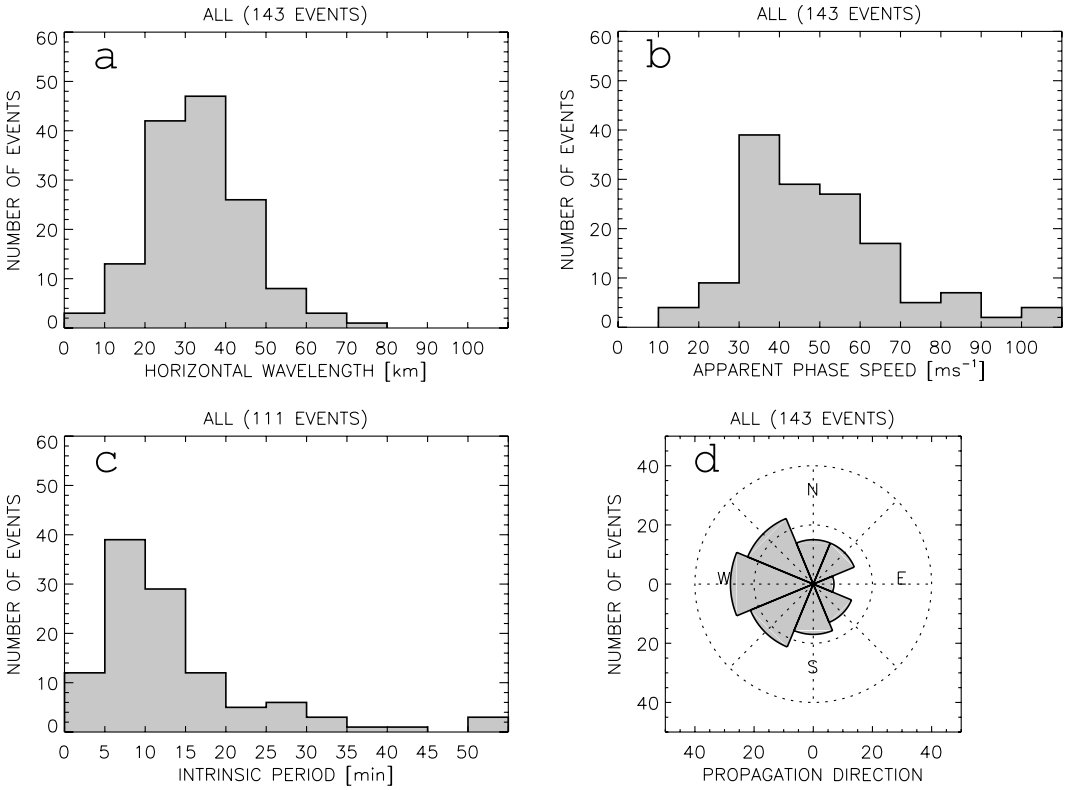

Figure 4. Histograms showing the distribution of the small-scale wave parameters. (a) Horizontal wavelength, (b) horizontal apparent (observed) phase speed, (c) intrinsic wave period, and (d) horizontal propagation direction.

to 29 November 2006. The uppermost (bottom) digit shown above each bar is the number of small-scale (large-scale) wave events. The wave parameters (horizontal wavelength, phase speed, and propagation direction) of each wave were generally observed to be steady for several hours. Out of the 211-night observations, 137 nights were clear and available for analysis. The ratio of clear-sky intervals to the total observations was 43% (914 hours/2150 hours). We found 143 small-scale and 61 large-scale wave events during the clear-sky intervals. A meteor radar collocated at the Resolute Bay optical site simultaneously observed wind at MLT heights (82–98 km for ~3 km and 2-hourly averages) [*Hocking*, 2001; *Hocking et al.*, 2001] for almost all the nights for which the wave events were obtained (111 out of 143 small-scale wave events and 49 out of 61 large-scale wave events). These MLT winds, which were observed simultaneously with the wave events, allow us to calculate the intrinsic parameters of the observed waves in the airglow images.

3. Statistical Results

[12] Figure 4 presents a summary of the wave parameters of the 143 small-scale wave events. Horizontal wavelength (Figure 4a), apparent (observed) horizontal phase speed c (Figure 4b), and intrinsic wave period $\tau(=\lambda_h/|c-u|$, where u is the wind speed along the wave propagation direction at 90 km) (Figure 4c), were mainly distributed in the bands 20–50 km, 30–60 ms^{-1}, and 5–15 min, respectively. These distributions are typical of those obtained by the other imaging observations at middle and low latitudes [e.g., *Taylor et al.*, 1997; *Nakamura et al.*, 1999, 2003; *Suzuki et al.*, 2004]. Figure 4d shows the horizontal propagation direction of the waves. The observed waves propagated predominantly westward (SW, W, and NW, with a peak of W) and were less likely to propagate eastward. This characteristic pattern of the propagation direction will be discussed in the next section.

[13] We also determined whether the waves propagated freely or were ducted. The vertical wave numbers m of the 111 events with simultaneous meteor wind measurements were calculated from the approximate linear dispersion relation for gravity waves

$$m^2 = \frac{N^2}{(c-u)^2} - k^2 - \frac{1}{4H}, \tag{1}$$

where N is the Brunt-Väisälä frequency, $k(=2\pi/\lambda_h)$ is the horizontal wave number, and H is the density scale height. At the MLT height, N and H are typically 0.02 rad s^{-1} and 6 km, respectively [*Suzuki et al.*, 2007]. We found that 14 events (13%) exhibited ducted or evanescent behaviors ($m^2 < 0$). Note, the sign of m^2 is sensitive to the first term in equation (1). Therefore this ducting rate may be limited slightly by the fact that the meteor winds were made only at a resolution of 3 km with 2 hourly.

[14] Figure 5 shows the parameters of large-scale waves (61 events) in the same manner as Figure 4. Horizontal wavelength, apparent phase speed, and intrinsic wave period

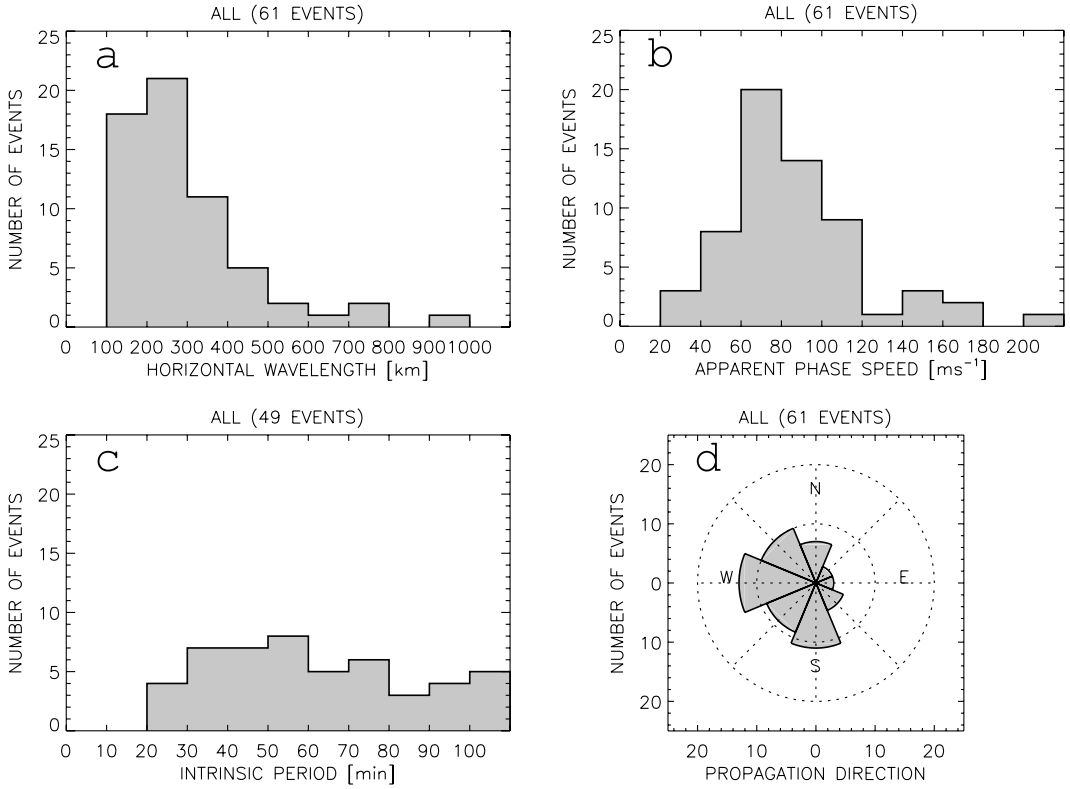

Figure 5. Same as Figure 4 but for the large-scale waves obtained from keograms.

were mainly distributed within the bands of 100–400 km, 60–100 ms^{-1}, and 30–80 min, respectively. The distribution of the horizontal propagation directions for large-scale waves was similar to that of the small-scale waves, as shown in Figure 4d, i.e., predominantly westward and less eastward. However, the net southward propagation of large-scale waves was slightly enhanced relative to that of the small-scale waves. Figure 5a shows that all the large-scale waves had horizontal wavelengths greater than 100 km, while the horizontal wavelengths of the small-scale waves were less than 100 km (see Figure 4a). This fact indicates that the small-scale and large-scale waves were distinguished, without overlap, by two different image processing schemes (consecutive images and keograms).

[15] Using equation (1) together with the MLT meteor wind measurements, we found that all the observed large-scale waves (49 events) propagated freely ($m^2 > 0$). This is probably due to their greater horizontal wavelengths, and hence smaller k, which are more likely to lead positive m^2 in equation (1).

4. Discussion

[16] In this section, we discuss the possible sources of the observed polar cap gravity waves. *Smith et al.* [2000] reported that there was no clear evidence of small-scale gravity waves generated by auroral processes on the basis of 12 nights of airglow imaging observation at a subauroral latitude of Millstone Hill (geomagnetic latitude: 53.0°N). If auroral activity is a wave source and the induced gravity waves are observable in the mesospheric airglow images, the waves propagating equatorward would be dominant at the subauroral sites, especially during periods of high geomagnetic activity. However, most of the observed waves exhibited poleward motion even for active geomagnetic conditions ($K_p > 3$).

[17] In a similar manner, we investigated whether the polar cap gravity waves extracted in the present analysis were induced by auroral energy deposition in the upper atmosphere. All gravity wave events were divided into two groups according to geomagnetic conditions during each wave event. One group corresponded to the active phase ($K_p > 3$) and the other to the quiet phase ($K_p < 3$). The former group contained 23 (9) events of small-scale (large-scale) waves and the latter contained 87 (38) events. Note that, active and quiet geomagnetic periods constituted 16% and 62%, respectively, of all the clear-sky observation periods. In the distributions of wave parameters (horizontal wavelengths, apparent phase speeds, and intrinsic wave periods), no significant changes caused by geomagnetic activity were identified. Even for the active conditions, we did not detect any systematic directionality in the wave propagation, which would have implied auroral sources (not shown). Thus our study negates that the polar cap gravity waves were associated with auroral activities.

[18] We now discuss the possibility of wave sources being present in the lower atmosphere. Meteorological dynamics in the lower atmosphere are often considered to be the main source of MLT gravity waves. Gravity waves generated in the lower atmosphere and propagating upward cannot pass through the critical level height, where their horizontal phase velocity becomes equal to the background horizontal wind velocity component along the wave phase speed vector, and the vertical wavelength becomes zero in equation (1). This

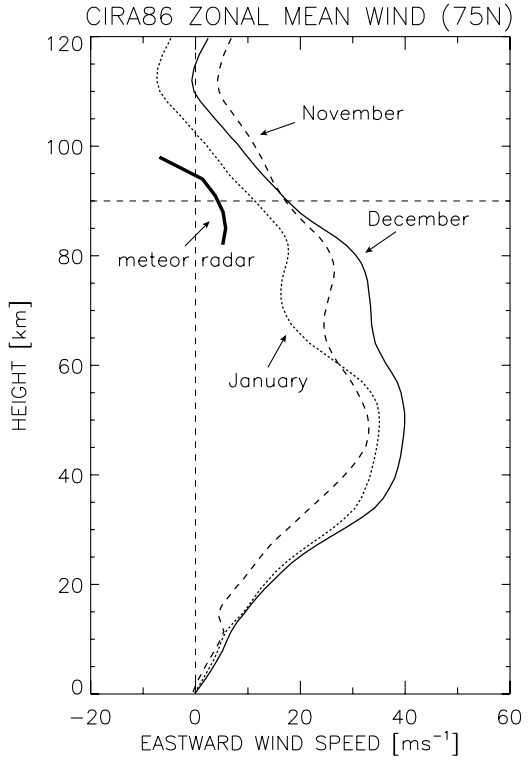

Figure 6. Zonal wind profiles at 75°N from the CIRA-86 model for November (dashed curve), December (solid curve), and January (dotted curve). The meteor wind data averaged for all the observed gravity wave events are indicated by the thick solid curve between 82 and 98 km. The vertical and horizontal dashed lines show the zero of the zonal wind and the sodium airglow layer height of 90 km, respectively.

is the concept of critical-level filtering [*Taylor et al.*, 1993, and references therein]. Only the gravity waves with phase velocity greater than the peak underlying background wind velocity, or whose direction is opposite to the background wind, can reach the upper atmosphere.

[19] Figure 6 shows the CIRA-86 zonal wind profiles at 75°N, near the Resolute Bay site, in the winter months (November, December, and January). The observed meteor wind at the MLT heights (82–98 km), which was averaged for all the wave events, is shown by a heavy solid curve. The zonal winds are predominantly eastward from the lower atmosphere up to the sodium layer height (90 km, as indicated by the horizontal dashed line). They reach ~40 ms^{-1} in the upper stratosphere and lower mesosphere at altitudes of 40–60 km. These eastward-dominated wind conditions below the airglow height are consistent with the directions observed for gravity wave propagation, which are less frequently eastward, in terms of the wind filtering.

[20] If the observed gravity waves in the airglow images were generated in the lower atmosphere and survived the filtering by the eastward wind field, the eastward waves observed in the sodium images should have had a phase speed greater than the underlying wind velocities. Figure 7 shows the polar histogram of small-scale gravity waves (light grey hatched, same as Figure 4d), overplotted on the histogram of the waves having a phase speed greater than 40 ms^{-1} (dark grey hatched). For the waves with westward components (NW, W, and SW), the occurrence rate of waves with a greater phase speed (c > 40 ms^{-1}) was 52%. On the other hand, for the waves with eastward components (NE, E, and SE), the waves with a greater phase speed were dominant (83%). These facts are the evidence that the gravity waves undergo the filtering by the eastward wind, shown in Figure 6, through their upward propagation. That is, in the case of westward propagation, the gravity waves reach the airglow height irrespective of their phase speed. In contrast, for the eastward propagation, the waves with a greater phase speed can survive.

[21] At the middle and low latitudes, several studies reported gravity waves generated by tropospheric convection near the observation sites [e.g., *Nakamura et al.*, 2003; *Suzuki et al.*, 2007; *Wrasse et al.*, 2006; *Taylor and Hapgood*, 1988]. Figure 8 shows the averaged horizontal distributions of vertical pressure velocity (Omega) and geopotential height at two heights of 100 and 200 hPa from the NCEP Reanalysis data. A positive (negative) vertical velocity indicates downward (upward) motion of air mass and a lower geopotential height corresponds to lower pressure.

[22] The figure indicates that when the gravity waves were observed, the upper trough was most probably located to the east of the observation site. In the mature stage of the midlatitude depression, an updraft appeared near the center of the depression and convection was associated with the depression. These conditions are consistent with the propagation directions of the observed waves, which predominantly propagate westward. The low-pressure area was more likely to distribute to the northeast of the site. This is again consistent with the slight southward preference of wave propagations. It is presumable that when such a trough/ridge axis existed a lot of time here, the unbalanced jet-exit winds would be also a continual wave source.

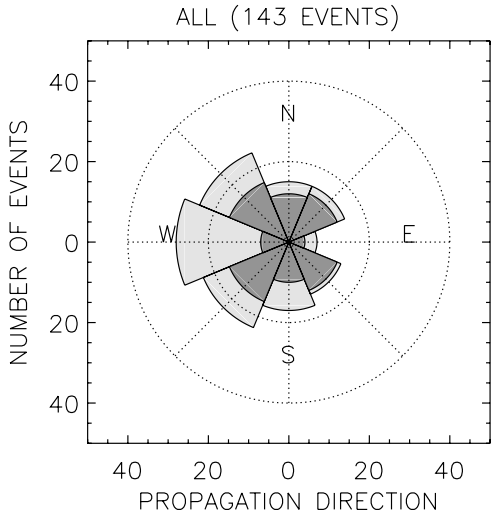

Figure 7. Same as Figure 4d except for overplotting the distribution of small-scale gravity waves that have a phase speed greater than 40 ms^{-1} (dark grey) on the histogram of all 143 small-scale waves (light grey).

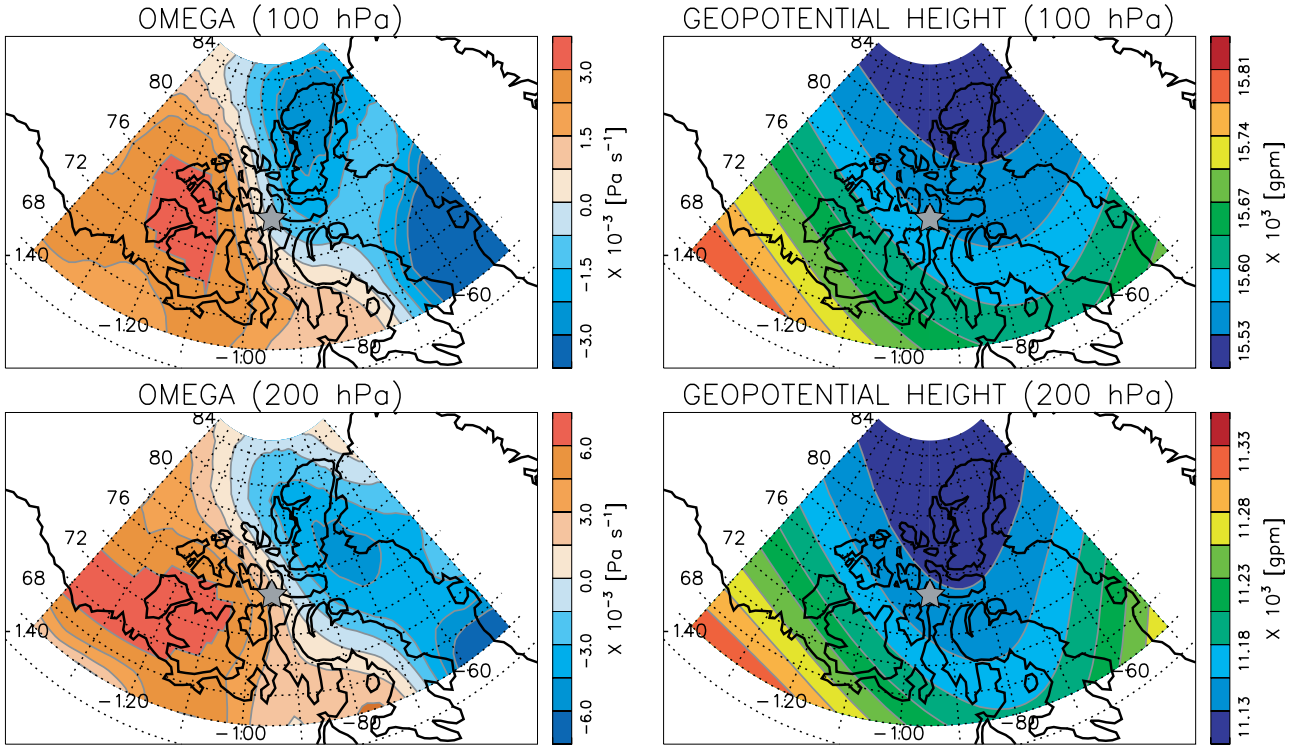

Figure 8. Horizontal distributions of the (left) Omega parameter and (right) geopotential height from the NCEP Reanalysis data at the heights of (top) 100 and (bottom) 200 hPa. These values are averaged for the months over which gravity waves were observed. The grey stars indicate the location of Resolute Bay.

[23] Thus the wind fields in the middle atmosphere and the atmospheric conditions in the lower atmosphere suggest that the gravity waves identified in the sodium airglow images mainly originated in the troposphere.

5. Summary and Conclusion

[24] In this study, we have reported statistics relating to the polar cap mesospheric gravity waves obtained at Resolute Bay (74.7°N) based on the sodium airglow imaging observations for 137 clear nights in the winter months of 2005 and 2006. We identified large-scale gravity waves (61 events) using airglow keograms as well as small-scale gravity waves (143 events), which were directly identified in the FOV of airglow images (256 km × 256 km in this paper). The statistical wave characteristics are summarized as follows.

[25] 1. The observed small-scale gravity waves mainly have a horizontal wavelength of 20–50 km, an apparent phase speed of 30–60 ms^{-1}, and an intrinsic wave period of 5–15 min.

[26] 2. The observed large-scale gravity waves mainly have a horizontal wavelength of 100–400 km, an apparent phase speed of 60–100 ms^{-1}, and an intrinsic wave period of 30–80 min.

[27] 3. The propagation directions of both type of wave are very similar; with westward dominating and eastward being less common.

[28] 4. There is no clear relation between the gravity wave parameters and the auroral activity. However, the propagation directions of the waves are in good agreement with the wind fields in the middle atmosphere and with the atmospheric conditions in the lower atmosphere. These results suggest that the polar cap mesospheric gravity waves observed at Resolute Bay are generated by tropospheric dynamics rather than the auroral processes.

[29] We also notice that, in this paper, we used a zonal mean wind model and averaged field of the lower atmosphere. Therefore the next step is to investigate in detail a correlation between the observed gravity wave features and individual weather system properties, since the atmospheric condition at high latitudes is often distorted with such as the disturbed polar vortex and stratospheric warming.

[30] **Acknowledgments.** We gratefully acknowledge T. Katoh, Y. Katoh, and M. Satoh of the Solar-Terrestrial Environment Laboratory, Nagoya University, for their skillful support in the airglow measurements. This work was supported by a Grant-in-Aid for Scientific Research (16403007, 19403010, and 20244080) of the Ministry of Education, Culture, Sports, Science and Technology of Japan. W.K.H. was supported by the Natural Sciences and Engineering Research Council of Canada. We are grateful to SRI International, and especially to John Kelly, for supporting the observation site. The optical observation at Resolute Bay was supported by the NSF cooperative agreement ATM-0608577. NCEP Reanalysis data were provided by the NOAA/OAR/ESRL PSD, Boulder, Colorado, USA, from their Web site at http://www.cdc.noaa.gov/.

[31] Amitava Bhattacharjee thanks Peter Dyson and Stephen Eckermann for their assistance in evaluating this paper.

References

Espy, P. J., G. O. L. Jones, G. R. Swenson, J. Tang, and M. J. Taylor (2004), Seasonal variations of the gravity wave momentum flux in the Antarctic mesosphere and lower thermosphere, *J. Geophys. Res.*, *109*, D23109, doi:10.1029/2003JD004446.

Ejiri, M. K., K. Shiokawa, T. Ogawa, K. Igarashi, T. Nakamura, and T. Tsuda (2003), Statistical study of short-period gravity waves in OH

and OI nightglow images at two separated sites, *J. Geophys. Res.*, *108*(D21), 4679, doi:10.1029/2002JD002795.

Fritts, D. C., and M. J. Alexander (2003), Gravity wave dynamics and effects in the middle atmosphere, *Rev. Geophys.*, *41*(1), 1003, doi:10.1029/2001RG000106.

Hocking, W. K. (2001), Middle atmosphere dynamical studies at Resolute Bay over a full representative year: Planetary waves, tides and special oscillations, *Radio Sci.*, *36*, 1795–1822.

Hocking, W. K., M. C. Kelley, R. Rogers, W. O. J. Brown, D. Moorcroft, and J.-P. St. Maurice (2001), Resolute Bay VHF radar: A multi-purpose tool for studies of tropospheric motions, middle atmosphere dynamics, meteor physics and ionospheric physics, *Radio Sci.*, *36*, 1839–1857.

Hosokawa, K., K. Shiokawa, Y. Otsuka, A. Nakajima, T. Ogawa, and J. D. Kelly (2006), Estimating drift velocity of polar cap patches with all-sky airglow imager at Resolute Bay, Canada, *Geophys. Res. Lett.*, *33*, L15111, doi:10.1029/2006GL026916.

Jiang, J. H., S. D. Eckermann, D. L. Wu, and J. Ma (2004), A search for mountain waves in MLS stratospheric limb radiances from the winter Northern Hemisphere: Data analysis and global mountain wave modeling, *J. Geophys. Res.*, *109*, D03107, doi:10.1029/2003JD003974.

Lindzen, R. S. (1981), Turbulence and stress owing to gravity wave and tidal breakdown, *J. Geophys. Res.*, *86*, 9707–9714.

Nakamura, T., A. Higashikawa, T. Tsuda, and Y. Matsushita (1999), Seasonal variations of gravity wave structures in OH airglow with a CCD imager at Shigaraki, *Earth Planets Space*, *51*, 897–906.

Nakamura, T., T. Aono, T. Tsuda, A. G. Admiranto, E. Achmad, and Suranto (2003), Mesospheric gravity waves over a tropical convective region observed by OH airglow imaging in Indonesia, *Geophys. Res. Lett.*, *30*(17), 1882, doi:10.1029/2003GL017619.

Shiokawa, K., Y. Katoh, M. Satoh, M. K. Ejiri, and T. Ogawa (1999), Development of optical mesosphere thermosphere imagers, *Earth Planets Space*, *51*, 887–896.

Shiokawa, K., Y. Otsuka, and T. Ogawa (2009), Propagation characteristics of nighttime mesospheric and thermospheric waves observed by optical mesosphere thermosphere imagers at middle and low latitudes, *Earth Planets Space*, in press.

Smith, S. M., M. Mendillo, J. Baumgardner, and R. R. Clark (2000), Mesospheric gravity wave imaging at a subauroral site: First results from Millstone Hill, *J. Geophys. Res.*, *105*, 27,119–27,130.

Suzuki, S., K. Shiokawa, Y. Otsuka, T. Ogawa, and P. Wilkinson (2004), Statistical characteristics of gravity waves observed by an all-sky imager at Darwin, Australia, *J. Geophys. Res.*, *109*, D20S07, doi:10.1029/2003JD004336.

Suzuki, S., K. Shiokawa, Y. Otsuka, T. Ogawa, K. Nakamura, and T. Nakamura (2007), A concentric gravity wave structure in the mesospheric airglow images, *J. Geophys. Res.*, *112*, D02102, doi:10.1029/2005JD006558.

Swenson, G. R., and S. B. Mende (1994), OH emission and gravity waves (including a breaking wave) in all-sky imagery from Bear Lake, UT, *Geophys. Res. Lett.*, *21*, 2239–2242.

Tang, J., G. R. Swenson, A. Z. Liu, and F. Kamalabadi (2005), Observational investigations of gravity wave momentum flux with spectroscopic imaging, *J. Geophys. Res.*, *110*, D09S09, doi:10.1029/2004JD004778.

Taylor, M. J., and M. A. Hapgood (1988), Identification of a thunderstorm as a source of short period gravity waves in the upper atmospheric nightglow emissions, *Planet. Space Sci.*, *36*, 975–985.

Taylor, M. J., E. H. Ryan, T. F. Tuan, and R. Edwards (1993), Evidence of preferential directions for gravity wave propagation due to wind filtering in the middle atmosphere, *J. Geophys. Res.*, *98*, 6047–6057.

Taylor, M. J., M. B. Bishop, and V. Taylor (1995), All-sky measurements of short period waves imaged in the OI (557.7 nm), Na (589.2) and near infrared OH and O_2 (0, 1) nightglow emissions during the ALOHA-93 campaign, *Geophys. Res. Lett.*, *22*, 2833–2836.

Taylor, M. J., W. R. Pendleton Jr., S. Clark, H. Takahashi, D. Gobbi, and R. A. Goldberg (1997), Image measurements of short-period gravity waves at equatorial latitudes, *J. Geophys. Res.*, *102*, 26,283–26,299.

Walterscheid, R. L., J. H. Hecht, R. A. Vincent, I. M. Reid, J. Woithe, and M. P. Hickey (1999), Analysis and interpretation of airglow and radar observations of quasi-monochromatic gravity waves in the upper mesosphere and lower thermosphere over Adelaide, Australia (35°S, 138°E), *J. Atmos. Terr. Phys.*, *61*, 461–478.

Wrasse, C. M., et al. (2006), Reverse ray tracing of the mesospheric gravity waves observed at 23°S (Brazil) and 7°S (Indonesia) in airglow imagers, *J. Atmos. Terr. Phys.*, *68*, 163–181.

W. K. Hocking, Department of Physics and Astronomy, University of Western Ontario, 1151 Richmond Street North, London, ON N6A 3K7, Canada. (whocking@uwo.ca)

K. Hosokawa, Department of Information and Communication Engineering, University of Electro-Communications, Chofugaoka 1-5-1, Chofu, Tokyo 182-8585, Japan. (hosokawa@ice.uec.ac.jp)

K. Nakamura, Hydrospheric Atmospheric Research Center, Nagoya University, Nagoya, Aichi 464-8601, Japan. (nakamura@hyarc.nagoya-u.ac.jp)

K. Shiokawa, Solar-Terrestrial Environment Laboratory, Nagoya University, Nagoya, Aichi 464-8601, Japan. (shiokawa@stelab.nagoya-u.ac.jp)

S. Suzuki, Sugadaira Space Radio Observatory, University of Electro-Communications, Chofugaoka 1-5-1, Chofu, Tokyo 182-8585, Japan. (shin.s@ice.uec.ac.jp)